Absolute vibrational excitation cross sections for slow-electron (1–18 eV) scattering in solid H_2O

M. Michaud and L. Sanche
Groupe du Conseil de Recherches Médicales en Sciences des Radiations, Faculté de Médecine, Université de Sherbrooke, Sherbrooke, Quebec, Canada J1H 5N4
(Received 26 May 1987)

High-resolution vibrational electron-energy-loss spectra of amorphous ice films condensed at 14 K are reported for the incident-energy range 1–18 eV. Absolute electron scattering cross sections for elastic collisions, individual vibrational excitations, and the sum of electronic transitions are obtained by performing a two-stream multiple-scattering analysis of the spectra. The various features found in the energy-dependent cross sections are discussed, whenever possible, by comparison with data and mechanisms (e.g., transient anion formation) well established in the gas phase. Quantum-interference effects introduced implicitly in the cross sections by the classical analysis are discussed within the first Born approximation for electron–multiple-site scattering.

I. INTRODUCTION

The interaction of an electron with condensed matter can be characterized through the knowledge of electron scattering cross sections or related mean free paths (MFP's) for energy transfer to various excitation modes of a medium.[1] The determination of the energy dependence of these cross sections particularly at low energy (i.e., less than 100 eV) permits the identification of scattering mechanisms contributing to specific electron-energy deposition and transport processes in the condensed phase.[2,3] In the solid phase, information on electron scattering cross sections can be most directly obtained by performing electron-beam experiments[4] similar to those in the gas phase.[5] Accordingly, a series of high-resolution electron-energy-loss (HREEL),[6–8] low-energy electron transmission (LEET),[7–10] and electron-stimulated desorption[11] experiments have been performed on multilayer molecular films condensed on cold metal substrates. Relying particularly on electron inelastically backscattered intensities to infer scattering mechanisms, we have identified the formation of transient negative ion (i.e., anion) states or electron resonances by qualitative comparison with gas-phase cross sections.[6] However, when the thickness of a molecular film is of the order of the electron mean free path (MFP) or greater, the resulting backscattered and transmitted intensities are subjected to plural scatterings. Moreover, new nuclear as well as electronic excitation modes can arise in the solid phase, and also the molecular building blocks can be difficult if not impossible to isolate for comparison in the gas phase. Therefore, appropriate expressions including multiple-scattering effects are needed in order to interpret in a straightforward manner the experimental results. Since it is not obvious how to carry through a microscopic description in complete generality, current analyses rely either on quantum[4,12] or classical models.[9,13–17] Generally, these include particular simplifications adapted to what is believed to be important for a reasonable description of the data.

In a previous paper[14] (henceforth referred to as I), we derived an analytical expression which relates the scattering probability per unit length (SPUL) or cross section per scatterer to the energy distribution of backscattered electrons as a function of the thickness of a solid film. This expression is particularly suitable if electrons scatter incoherently from a disordered molecular film and if the excitation of various nuclear vibrational modes is the phenomenon investigated. It served to analyze librational and intramolecular-vibrational excitations produced by 1–30-eV electrons incident on multilayer N_2 and CO films.[6] In a more recent work[16] we used the same framework to relate by a simple analytical expression the thickness dependence of the elastic electron reflectivity of a molecular film to the absolute value of the total effective and total inelastic scattering cross section per scatterer. The proposed method was then applied to extract from high-resolution elastic scattering measurements on amorphous ice films condensed at 14 K, the total electron scattering cross sections in the 1–20-eV range.[16]

The purpose of the present paper is to show how, with the knowledge of the total cross sections, specific electron scattering cross sections or SPUL for energy transfer to a medium can be extracted from HREEL spectra recorded at high film thickness. We extend our earlier work on amorphous ice films[16] in extracting scattering cross sections for nuclear and electronic excitations in the 1–18-eV range. To this end HREEL spectra of thick ice films (i.e., 30 layers) are recorded for several incident energies. Then, with the multiple-scattering model developed in I for a semi-infinite medium, the spectra are numerically fitted to determine the relative magnitude of the cross sections (i.e., with respect to the total). Finally, by normalizing these to the total effective cross section, the energy dependence of electron scattering cross sections for the major energy-loss processes are obtained.

This paper is organized in the following manner. In Sec. II we recall the main steps of the two-stream

multiple-scattering model developed in I and give the physical interpretation behind the parameters. The experimental conditions for a suitable application of this model are stated and verified in the case of condensed H_2O films in Sec. III. In Sec. IV HREEL spectra of amorphous ice films as well as the excitation functions for the major energy losses are presented. In Sec. V the numerical procedure is explained and the results of the analysis are given. The various features found in the cross sections are then discussed and compared with gas-phase data in Sec. VI.

II. THE TWO-STREAM MODEL

At low energy, the interaction of an electron with the various nuclear and electronic excitation modes of matter results in real excitations (i.e., transfer of energy) and virtual excitations (i.e., energy-forbidden transitions allowed by the uncertainty principle). The excitation modes can then be classified with respect to the incident electron energy (E_0) as open or closed scattering channels. The effect of the electronic excitation modes on multiple scattering inside the film is taken into account by the renormalization of the electron energy or wave vector in introducing a generalized optical potential or electron self-energy.[18] Microscopically, this is usually an energy-dependent and nonlocal operator, which reduces for an isolated molecule at long range to the polarization interaction potential. Owing to the overlapping of these interaction potentials in a condensed medium, an energy-dependent but spatially constant complex potential (i.e., $V_p+i\Gamma$) can be introduced as a first approximation.[19] The imaginary part (Γ) is related to the total inelastic SPUL (α_i) pertaining to the open electronic channels via $\Gamma=\alpha_i(\hbar^2/m)[(2m/\hbar^2)(-V_p+E_0)]^{1/2}$,[20] where m is the mass of the electron. The real part (V_p) (Ref. 21) is more specifically considered here as the average over a unit volume or cell occupied by a molecule of the screened electron-molecule electronic polarization potential originating from all other cells (i.e., the long-range part). It is expected to match an imagelike potential outside the solid and is responsible for the film-vacuum potential barrier experienced by ingoing as well as outgoing electrons. The multiple scattering originating from the short-range part of the polarization interaction and from the static-exchange interaction is described by a classical transfer equation which includes various cross sections pertaining to the open channels.

The central idea in the classical approach is that due to molecular disorder and incoherent inelastic scattering, a cross section or SPUL can be defined for an effective volume beyond which electron interferences and correlation effects (i.e., between these volumes) can be neglected. A more formal description which sheds light on this concept has been presented recently by Fano and Stephens,[22] who draw a line between the quantum and classical behavior of electron scattering in amorphous condensed matter. They introduce and define specifically, for an electron of incident energy ε, a stochastic element of probability $k_\varepsilon(\mathbf{q},\omega)$ for energy $\hbar\omega$ and momentum $\hbar\mathbf{q}$ transfer per unit path length suitable for the Boltzmann transfer equation. In the context where the first Born approximation is valid, this quantity is proportional to the product of the dynamical structure factor by a form factor. In the absence of any correlation between sites (e.g., in the gas phase) this definition reduces to the product of the individual cross section by the density of the medium.

Relying on the above considerations, we devised in I a solution for the electron multiple-scattering problem in two separate parts. The first part is aimed at calculating, the "intrinsic" backscattered energy-distribution intensity generated by incoherent multiple scattering resulting in real excitations of the nuclear vibrational modes in the film without the effect of the film-vacuum potential barrier. The second part estimates the effect of the barrier on the outgoing intensity.

The expression describing the intrinsic scattering part is based on the solution of the classical transfer equation for plane-parallel problems in the two-stream approximation [i.e., Eqs. (7) in I henceforth referred to as I.7] and characterizes a medium by various electron SPUL's. In the present context an electron SPUL to loose an energy $E-E'$ can be identified as $\int k_\varepsilon(\mathbf{q},\omega)d\mathbf{q}\equiv Q_t(E-E')$, where the integration is performed over the entire angular space for a fixed $\hbar\omega$. Moreover, $E'-E\equiv\hbar\omega$ is the transferred energy, with E' and E the incident and final electron energy with respect to the vacuum level, respectively. In I, the possible anisotropy of a scattering event is taken into account by splitting $Q_t(E-E')$ into an isotropic (i.e., large-angle) component $Q_r(E-E')$ and a forward (i.e., small-angle) component $Q_f(E-E')$ according to

$$Q_t(E-E')=2Q_r(E-E')+Q_f(E-E') . \tag{2.1}$$

If we define a coefficient of angular anisotropy γ, these latter components read

$$Q_f(E-E')=Q_t(E-E')\gamma(E-E') \tag{2.2a}$$

and

$$Q_r(E-E')=Q_t(E-E')[1-\gamma(E-E')]/2 . \tag{2.2b}$$

For small variation of the SPUL with incident energy in the energy-loss range of interest, we show in I that the application of the Fourier transform to the transfer equations (I.7) with appropriate boundary conditions yields the expressions (I.10) with (I.9) for the backscattered current-density distribution as a function of the film thickness. In the "limit" of a semi-infinite medium, this solution reduces to the expression (I.12), i.e.,

$$J_\infty(0,E)=\frac{1}{2\pi}\int_{-\infty}^{+\infty} I(0,s)R_\infty(0,s)\exp(-isE)ds , \tag{2.3a}$$

where

$$R_\infty(0,s)=\frac{1-Q_r(s)/\beta(s)-[1-2Q_r(s)/\beta(s)]^{1/2}}{Q_r(s)/\beta(s)} \tag{2.3b}$$

and $\beta(s)\equiv\alpha-Q_f(s)$. In (2.3a), $I(0,s)$ is the Fourier transform of the incident current distribution and yields a constant I_0 for a δ-distribution. In (2.3b), $R_\infty(0,s)$

represents the Fourier transform of the intrinsic reflectivity distribution at the film surface (i.e., position 0) with $Q_{r,f}(s)$ defined by the relation

$$Q_{r,f}(E-E')=\frac{1}{2\pi}\int_{-\infty}^{+\infty} Q_{r,f}(s)\exp[-is(E-E')]ds \ .$$

Finally, α is the total SPUL or inverse MFP given by

$$\alpha\equiv\int_{-\infty}^{+\infty}[2Q_r(E-E')+Q_f(E-E')]dE$$
$$=2Q_r(s=0)+Q_f(s=0) \ . \tag{2.4}$$

At high thickness, the resulting backscattered current-density distribution is no more dependent on the thickness of the film as well as the reflectivity of the substrate. Moreover, each SPUL component entering into Eqs. (2.3) is divided by the total SPUL α and can therefore be identified as a branching ratio. However, owing to our recently proposed method[16] which aims to extract directly $\alpha_{\text{eff}}\equiv\alpha-Q_{fe}$ instead of α, where $Q_{fe}\equiv Q_f(E=E')$ is the small-angle elastic SPUL, it becomes more appropriate in the present work to have SPUL values expressed relatively to α_{eff}. Using the above definition for $\beta(s)$, this transformation is easily made by replacing each ratio $Q_r(s)/\beta(s)$ in (2.3b) by

$$Q_r(s)/\beta(s)=[Q_r(s)/\alpha_{\text{eff}}]\{1/[1-Q_{fi}(s)/\alpha_{\text{eff}}]\} \ , \tag{2.5}$$

where $Q_{fi}(s)\equiv Q_f(s)-Q_{fe}$.

In the second part of the calculation the film-vacuum potential barrier originating from V_p is taken into account by introducing a transmission coefficient (T) at a potential-barrier interface. T represents more specifically the fraction of outgoing electrons which are allowed by energy- and momentum-conservation laws (i.e., Snell-Descartes law) to escape the film-vacuum potential barrier.[23] This fraction reduces for the case of isotropic backscattering to

$$T=1-[V_p/(V_p-E)]^{1/2} \quad \text{for } E>0 \tag{2.6a}$$

and

$$T=0 \quad \text{for } E<0 \ . \tag{2.6b}$$

With respect to the vacuum level, V_p is expected to be a negative quantity and energy dependent, since it is related to the long-range part of the interaction potential pertaining to the electronic polarization. If T can be considered independent of the energy over a small (i.e., less than 1 eV) energy-loss range, then the outgoing backscattered current-density distribution $J_\infty^T(0,E)$ is given by expression (I.13), i.e.,

$$J_\infty^T(0,E)=\frac{1}{2\pi}\int_{-\infty}^{+\infty}\frac{I(0,s)TR_\infty(0,s)}{1-(1-T)R_\infty(0,s)}\exp(-isE)ds \ , \tag{2.7}$$

where $R_\infty(0,s)$ is given by (2.3b). This represents the intrinsic backscattered current-density distribution multiply reflected between the film and the potential-barrier interface. In practice calculations of the backscattered intensity can be implemented either in the Fourier space or in the energy space. For this latter case, the radical in (2.3b) and the denominator in (2.7) are expanded into a series of increasing order in the number of collisions and reflections, respectively.

Without making any detailed numerical calculations, the behavior of the scattered intensities as a function of the scattering parameters can be inferred from the knowledge of some particular analytical expressions which can be derived from (2.7). For instance, let us examine expressions related to the elastic intensity and then to the inelastic intensity originating from a single inelastic event by including the angular anisotropy as well as elastic multiple scattering. The main steps for the derivation of these expressions are given in the Appendix since it has not been made in complete generality in I.

Using definitions (2.2) for the coefficient of angular anisotropy and the corresponding definition for $\alpha_{\text{eff}}\equiv\alpha-\gamma_e Q_{te}$, where $\gamma_e\equiv\gamma(E=E')$ and $Q_{te}\equiv Q_t(E=E')$, the expression for the elastic intensity (A3) reads

$$J_{\infty e}^T=\frac{I_0TR_{\infty e}}{1-(1-T)R_{\infty e}} \ , \tag{2.8a}$$

where $R_{\infty e}$ is the intrinsic elastic reflectivity given by

$$R_{\infty e}=\frac{1-[1-(1-\gamma_e)Q_{te}/\alpha_{\text{eff}}]^{1/2}}{1+[1-(1-\gamma_e)Q_{te}/\alpha_{\text{eff}}]^{1/2}} \ . \tag{2.8b}$$

For the case $\gamma_e=0$ (i.e., $Q_{fe}=0$) this latter reduces to the expression (18) in I. Examination of expressions (2.8) teaches us that the elastic reflectivity is essentially linked to the presence of large-angle elastic scattering and is subjected to variations originating from α_{eff}. Conversely, the presence of any small-angle elastic component is transparent to the elastic reflectivity value.

The expression for the inelastic current (A8) when combined with definitions (2.2) reads

$$J_{\infty i}^T(0,E)=\frac{I_0T}{[1-(1-T)R_{\infty e}]^2}\left[\frac{Q_{ti}(E-E_0)}{2\alpha_i}\right]\times\left[1-\gamma_i(E-E_0)\left[\frac{1-R_{\infty e}}{1+R_{\infty e}}\right]^2\right]\times\left[\frac{1-R_{\infty e}^2}{2}\right] \ , \tag{2.9}$$

where $\alpha_i\equiv\alpha-Q_{te}=\alpha_{\text{eff}}-Q_{re}$ is the total inelastic SPUL, $Q_{ti}(E-E_0)\equiv Q_t(E-E_0)-Q_{te}$, $\gamma_i(E-E_0)\equiv\gamma(E-E_0)-\gamma_e$, and $R_{\infty e}$ is given explicitly by (2.8b). What was not obvious *a priori* and constitutes a key result from expression (2.9) is that the measured intensity of an inelastic feature, or even a change in that intensity, *does not necessarily reflect the value or a change in the SPUL or cross section.* In fact, the intensity of an energy-loss feature is expected to be proportional instead to the ratio of an inelastic SPUL to the total inelastic SPUL and be modulated by a factor of angular anisotropy. The effect of the transmission at the potential-barrier interface enters as a well-separated factor in (2.9). When expressed in terms of $R_{\infty e}$ elastic multiple scattering is seen to act as a particular factor $[(1-R_{\infty e})/(1+R_{\infty e})]^2$ renormalizing the coefficient of angular anisotropy γ_i, and as an additional factor $(1-R_{\infty e}^2)/2$ modulating the

overall inelastic intensity. Hence, with the knowledge of the intrinsic elastic reflectivity, one can readily estimate various effects due to elastic multiple scattering. For example, if variations in the intrinsic reflectivity are restricted to the range $R_{\infty e} \leq 0.3$, the modulating factor $(1-R^2_{\infty e})/2$ becomes nearly constant between 0.5 and 0.45. Alternatively, for the range $R_{\infty e} \geq 0.7$ the renormalizing factor $[(1-R_{\infty E})/(1+R_{\infty e})]^2$ reduces to less than 10% of the maximum effect of the angular anisotropy in the inelastic intensity.

III. EXPERIMENT

A. Apparatus

The measurements were performed with a HREEL spectrometer and a cryogenic target.[6] With respect to the outward normal of the target, the angle of incidence θ_0 of the monochromator can be varied from 14° to 70° and the angle of the analyzer θ_d is fixed at 45° at the opposite azimuth. The apparatus is housed in a cryopumped ultrahigh-vacuum system capable of sustaining working pressures around 5×10^{-11} torr.[24] In the present experiment, amorphous films of ice were grown from known quantities of triply distilled H_2O vapor condensed on a polycrystalline platinum substrate held at 14 K. The thickness was estimated *in situ* by monitoring on the substrate the transmitted current, previously calibrated with respect to the absolute H_2O coverage.[16] The incident current was 3×10^{-10} A for a combined resolution of 10 meV full width at half maximum (FWHM). The incident energy E_0 was calibrated within ±0.1 eV with respect to the vacuum level by measuring the onset of the transmitted current.

B. Experimental validation of the model

The purpose of the model exposed in Sec. II is to provide, by the introduction of simplifying assumptions, a tractable analysis of the backscattered electron intensity resulting from various incoherent multiple-scattering events in a condensed medium. Now let us describe the experimental conditions required to extract significant information from such analysis applied to HREEL spectra of multilayer molecular films deposited on a metal substrate.

The model is specially suited for disordered media. There is ample experimental evidence as mentioned in Ref. 16 that this condition is met for water condensed on a substrate held at 14 K. Moreover, the analysis focuses on the limit of a semi-infinite medium, where the reflectivity of the substrate can be neglected and the intensity of an energy-loss feature becomes independent of the film thickness. This implies that spectra must be recorded at the highest possible film thickness without creating observable charge buildup effects. Finally in the two-stream approximation, the detail of the angular distribution pertaining to a scattering event is neglected in favor of the introduction of a coefficient of angular anisotropy. Although this latter assumption cannot be justified on rigorous mathematical grounds, it suggests that the angular distribution of the measured backscattered intensity must be nearly isotropic and not peaked in the specular direction.

To illustrate all these considerations, we present in Fig. 1 the HREEL spectra of 15 layers of ice recorded for an incident energy of 3.2 eV at incident angles $\theta_0=14°$ and 45°. The energy-loss intensity at 45° is on the average 35% more intense than that at 14°. This is attributed in part in the geometrical configuration of the experiment and also to a small specular component of elastically and inelastically scattered intensities. As explained in I, when at the target, the object seen by the analyzer is greater than the area of the incident beam, the current collected by the analyzer becomes proportional, among other things, to the trigonometrical factor $1/(1+\cos\theta_0/\cos\theta_d)$. Thus, an increase of 20% in the collected intensity is expected *a priori* for θ_0 varying from 14° to 45°. On the other hand, the thickness dependence of the elastic and major inelastic peaks intensities in the specular direction for an incident energy of 7.2 eV are shown in the insert of Fig. 1. At low thickness, the open circles represent the intensity corrected for the background generated by the strong specular elastic peak. The solid curves were drawn to join smoothly the low- and high-thickness intensities. Owing to the effective dynamic dipole of the vibrational modes of the water molecules and also to the specular reflectivity of the substrate, the intensity of the energy losses increases until a maximum is reached around 2 to 3 layers.[25] At 12–15 layers, it is still possible to observe

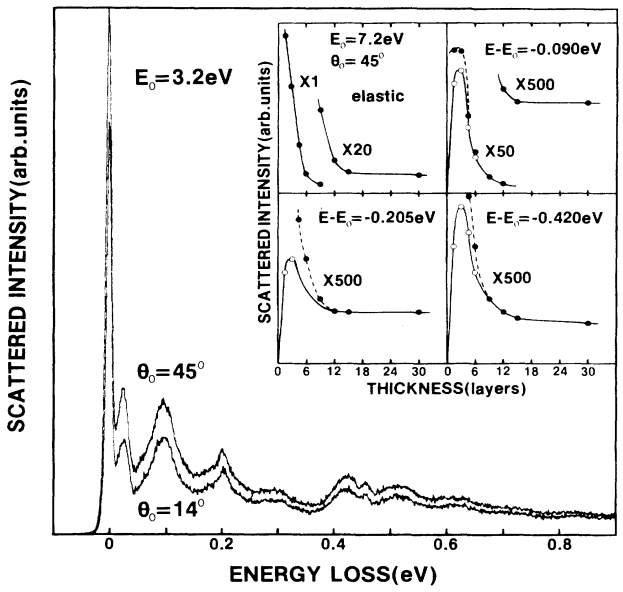

FIG. 1. Energy-loss spectra for 3.2-eV electrons incident on 15 layers of ice in the specular $\theta_0=45°$ and off-specular $\theta_0=14°$ directions. The difference in intensity is attributed mainly to the scattering geometry as explained in the text. The inset represents the thickness dependence of the elastic and major energy-loss peaks (i.e., $E-E_0$) recorded in the specular direction and for an incident energy of 7.2 eV. Above 15 layers, the intensity of an energy-loss features is almost independent of the thickness.

a small specular component. At higher thicknesses the intensity drops gradually to an essentially constant value comparable, within the effect of the geometrical factor, to the off-specular intensity.

In order to compare directly with the two-stream calculations, an absolute reflectivity scale must be established for all HREEL spectra by normalization to an effective incident current. This is obtained by a method which is described in detail in Ref. 16. Briefly, a HREEL spectrum recorded from threshold to the incident energy and the transmitted current are measured at a particular incident angle either for various incident energies or thicknesses. By plotting the transmitted current intensity as a function of the integrated HREEL spectra, a straight line is obtained whose intercept with the abscissa gives the effective incident current. As long as the angular distribution of the scattered intensity does not change appreciably with the incident energy or thickness, this procedure is expected to provide a reflectivity scale within an accuracy of $\pm 15\%$. In this manner, measurements performed on at least 30-layer amorphous ice films at 14° of incidence and 45° of analysis, once appropriately normalized, turn out to be *representative of a diffuse electron reflectivity of a semi-infinite sample* and suitable for a two-stream analysis in the limit of a semi-infinite medium.

IV. EXPERIMENTAL RESULTS

The dotted curves in Fig. 2 represent the vibrational energy-loss spectra of about 30 layers of H_2O deposited at 14 K and recorded at $\theta_0 = 14°$ and $\theta_d = 45°$ for several incident energies between 1.7 and 17.2 eV. The continuous curves represent the results of calculations discussed in Sec. V. Except for a higher background intensity resulting from multiple scattering, the spectra are similar to those obtained by other workers[26] in their investigations of H_2O adsorbed on various substrates.

The H_2O molecule in its ground state is bent and belongs to the C_{2v} point group.[27] The C_2 axis of rotation defines the z direction, the plane of the molecule lies in the xz plane, and the y direction is perpendicular to the plane of the molecule. The vibrations of H_2O in the gas phase are the bending mode (ν_2) found at 198 meV and the OH stretching modes divided into a symmetric stretch (ν_1) at 453 meV and an asymmetric stretch (ν_3) at 466 meV.[28]

By comparison with the infrared and Raman spectra of ice in its amorphous or crystalline form,[29–31] the main energy-loss features can be divided as those belonging to intermolecular vibrational (i.e., phonon) modes and those pertaining to intramolecular-vibrational modes of the free molecule. The peak at 25 meV, better resolved at low-incident energy, is ascribed to a translational phonon mode (ν_T) originating from frustrated translations of the free molecule. The large feature at 95–100 meV which separates into two structures at 95 and 65 meV around an incident energy of 9 eV is attributed to different librational phonon modes (ν_L). These can be considered as derived from the three frustrated rotations of the water molecules which under the crystal field and hydrogen bonding yield the large observed width.[30] Following the assignment of infrared spectra of ice I (Ref. 30) and Raman spectra of ice VIII,[31] we attribute the 65-meV feature to the superposition of librations of the molecule around the y and z directions and the 95-meV feature to librations in the x direction. The 205-meV loss peak and the large feature around 425 meV along with the small structure at 460 meV are ascribed to the bending mode ν_2 and the stretching modes $\nu_{1,3}$ of the water molecule, respectively. The maximum in the energy range of the stretching modes is observed to shift as function of the incident energy. At low and high energy it is located around 420 meV, whereas at 9 eV it is found around 430 meV. Owing to the fairly directional hydrogen bonding in the condensed phase, the bending mode becomes stiffer[32] and the stretching modes are lowered and broadened in energy mainly by the large distribution of bond restoring force constant resulting from local disorder.[33] Effects arising from Fermi resonance interaction[27] between the overtone of the bending mode ($2\nu_2$) at $\simeq 410$ meV and the symmetric stretch region are not expected to contribute significantly to the broadening.[33] Hence, the energy-loss shift of the stretch region can be attributed to a relative change between the contribution of the symmetric and asymmetric components to the scattering processes. Finally, the small and sharp peak at 460 meV corresponding closely to the gas-phase OH stretch is attributed to free OH oscillators which are not involved in hydrogen bonds,[34] particularly at the surface of the solid where energy broadening is expected to be minimal.

The energy dependence of the backscattered intensity (i.e., excitation function) for the elastic peak, and energy losses at $E - E_0 = 25$, 95, 205, and 425 meV corresponding to the intermolecular ν_T, ν_L and intramolecular $\nu_2, \nu_{1,3}$ vibrational modes, respectively, are shown by the dot-dashed curves in Fig. 3. These curves are derived from the HREEL spectra of Fig. 2. Continuous recordings of these excitation functions, but performed at a lower resolution (i.e., 25 meV FWHM) as shown for the elastic intensity on top of Fig. 3, indicate that the interval of 2 eV used is sufficient to represent their behavior. All excitation functions follow the same general trend and are characterized by two maxima around 5 and 12 eV. The excitation of the translational phonon mode ν_T increases relatively to the elastic intensity toward low energy. The minimum around 9 eV being less pronounced for the stretching modes $\nu_{1,3}$ than that for the other modes is an indication of a relative increase in the scattering probability for the excitation of these modes. This latter observation can be correlated with the energy-loss shift of the $\nu_{1,3}$ mode in this incident-energy range.

As shown by the multiple-scattering formulas of Sec. II, there is a certain ambiguity at this stage in sorting out from the excitation functions a well-defined behavior for the scattering probabilities, since the observed behaviors arise from the phenomenology involved as well as the overlap between energy-loss features. We develop in Sec. V a procedure based on the model of Sec. II in order to extract in a straightforward manner from HREEL

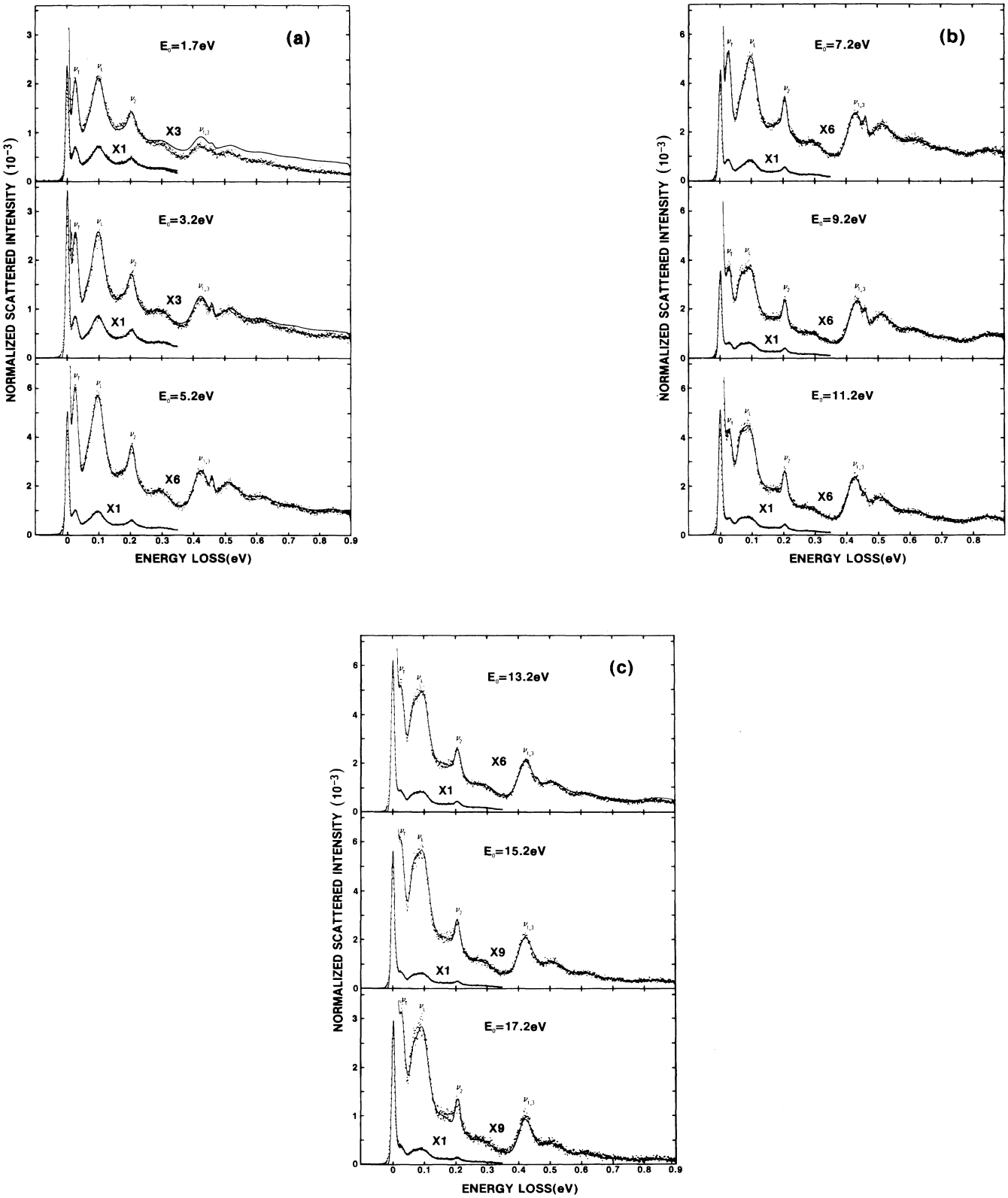

FIG. 2. Energy-loss spectra of 30-layer ice films for various incident energies. The dotted curves represent the normalized energy-loss spectra at an angle of incidence $\theta_0 = 14°$ and analysis $\theta_d = 45°$. The superimposed solid curves are the calculated energy distributions of backscattered electron resulting from a two-stream analysis of the spectra. The various parameters extracted from such analysis (e.g., cross sections) are listed in Table I. With the intensity scale, the integral of a feature can be expressed in terms of an elastic or inelastic absolute reflectivity.

spectra, the energy dependence of various electron scattering cross sections or SPUL values for vibrational excitations in amorphous ice.

V. TWO-STREAM ANALYSIS OF ICE

A. Fitting parameters

Owing to the large distribution of force constants for the various vibrational modes in amorphous ice, the relative SPUL are represented by a sum of Gaussian distribution functions as

$$Q_t(E-E')/\alpha_{\text{eff}}=\sum_i a_i \exp[-(E-E'+h\nu_i)^2/b_i^2] , \tag{5.1a}$$

with

$$b_i=\delta_i/[2(\ln 2)^{1/2}] , \tag{5.1b}$$

where a_i is the amplitude and δ_i the FWHM of a particular distribution centered around the excitation energy $h\nu_i$. The integral of a distribution $(Q_{t,i}/\alpha_{\text{eff}})$ represents the average relative SPUL pertaining to a given excitation mode ν_i and constitutes the key parameter. It is related to the amplitude and the width of the distribution by

$$Q_{t,i}/\alpha_{\text{eff}}=a_i b_i \pi^{1/2} . \tag{5.2}$$

Furthermore, each SPUL is characterized by the coefficient of angular anisotropy $(0\le\gamma_i\le 1)$ defined in (2.2), which allows Eqs. (5.1) to be separated into an isotropic component

$$Q_r(E-E')/\alpha_{\text{eff}} = \sum_i [(1-\gamma_i)/2]a_i \exp[-(E-E'+h\nu_i)^2/b_i^2] \tag{5.3a}$$

and a forward component

$$Q_f(E-E')/\alpha_{\text{eff}}=\sum_i \gamma_i a_i \exp[-(E-E'+h\nu_i)^2/b_i^2] . \tag{5.3b}$$

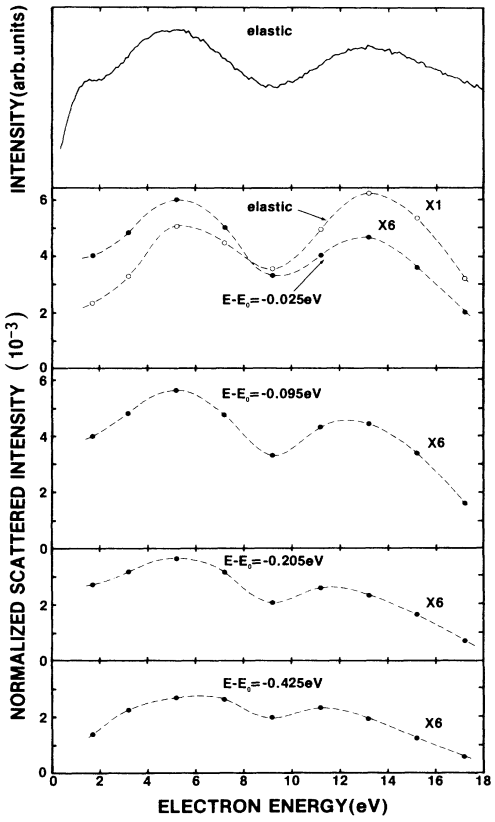

FIG. 3. Excitation functions for the elastic and major energy-loss features of 30-layer ice films recorded at an incidence angle $\theta_0=14°$. The top curve represents a continuous recording of the elastic peak obtained with a lower spectrometer resolution (i.e., 0.025 eV) whereas the dot-dashed curves are derived from the energy-loss spectra of Fig. 2. The energy losses $(E-E_0)$ at 0.025 eV, 0.095 eV, 0.205 eV, and 0.425 eV correspond to the vibrational modes ν_T, ν_L, ν_2, and $\nu_{1,3}$, respectively.

The potential-barrier transmission coefficient T is calculated via expressions (2.6) with V_p estimated along lines similar to the calculation of the relaxation energy of a negative ion embedded in a dielectric medium.[7] We consider for this estimate only the *electronic* polarization of ice with a dielectric constant $\epsilon=1.42$,[35] since the electron energy is greater than 1 eV in the experiments. For the fcc structure of ice[36] adjusted to the low-density amorphous form,[37] the relaxation energy amounts to 0.85 eV at the center of the Wigner-Seitz cell and 1.4, 1.6, and 1.9 eV at different points on its surface. These values represent an upper limit because the electron is treated as a point charge; they are expected to vary as the electron energy becomes comparable to the electronic excitation energy (i.e., greater than or equal to 7.5 eV).[38] They are also consistent with the value of the bottom of the conduction band which has been estimated at 0.9 eV below the vacuum level[39] from the ultraviolet-photoelectron threshold and the value of the band gap derived from the absorption edge. For the purpose of the two-stream analysis, we chose $V_p=-1$ eV and constant as a function of electron energy. As we verified by test calculations, a variation of ± 0.5 eV of this value proved to be insensitive within a constant factor to the relative fit of the reflected intensity. However, such a variation is determinant if we try to fit simultaneously the transmitted current.[17]

The finite energy resolution of the spectrometer is simulated in the last step of the calculation by convolution with suitable Gaussian distribution function.

B. Numerical procedure

Prior to the analysis, an absolute reflectivity scale is established for the HREEL spectra by normalization with an effective incident current as mentioned in Sec. III B. In this manner, the integral of an experimental feature yields an absolute reflectivity value appropriate

for comparison with the calculations. The generation of the backscattered energy distribution is performed with an energy mesh of 1 meV in order to compare as closely as possible with the experimental results. In a first approximation, the energy position and width of a Gaussian distribution SPUL is inferred from the experimental spectrum and refined as the calculation progresses. Thus, as a first step, the relative isotropic elastic SPUL (i.e., $2Q_{re}/\alpha_{\rm eff} \equiv (1-\gamma_e)Q_{te}/\alpha_{\rm eff}$) is obtained from the integral of the elastic peak using the inverse of expression (2.8). Then the full calculation of the backscattered energy distribution is performed via expression (2.7). According to the result of comparison with the experimental data, appropriate corrections are added. The preceding steps are repeated systematically from the elastic peak toward higher energy-loss features using the inverse of expression (2.9) to estimate the inelastic SPUL values. In the course of the calculation, it turns out that while some features necessitate the inclusion of additional SPUL, others can be accounted for by the multiple-scattering background. Finally, the entire analysis is resumed from one energy-loss spectrum to another with the constraint of consistency in the values and width of the energy losses.

C. Results of the analysis

In Fig. 2 we present the calculated energy distribution curves (solid line) superposed on their respective experimental spectra (dotted line). Except for the 1.7-eV result, the fit was performed until an agreement better than $\pm 5\%$ was achieved for the intensity of all features. For the 1.7-eV curve, the discrepancy at high-energy loss is mainly attributed to a decrease in the transmission of the analyzer lens at very low energy (i.e., less than 1 eV). The apparent disagreement between the measured and calculated elastic distribution results from the shape of the experimental distribution being larger at the base than a Gaussian function. In this case, we have compared the integral of the elastic peaks without attempting to fit exactly the distribution. Otherwise, all inelastic features could be easily reproduced with the set of parameters defined in Sec. V A. All the parameters corresponding to the calculated curves are listed in Table I. The relative SPUL associated with various excitation modes are included already normalized to the total effective cross section per scatterer (i.e., $\sigma_{T,\rm eff} \equiv \alpha_{\rm eff}/n$) which has been determined in Ref. 16 and where n is the bulk density of the medium. The energy variation of the various cross sections are illustrated in Fig. 4 for the purpose of discussion. Each error bar represents the sum of incertitudes resulting from the fit of Fig. 2 at $\pm 5\%$ and from the least-square-fit analysis (e.g., at an overall accuracy of $\pm 10\%$) leading to the total effective cross section.[16] It does not include the systematic incertitude at $\pm 25\%$ pendant to the extraction method and the coverage measurement.[16] As one can see, these curves differ from the excitation functions of Fig. 3 since now overlapping of the energy-loss peaks as well as the phenomenological effects due to incoherent multiple scattering are removed. However, the cross sections so extracted include intrinsically quantum effects pertaining to a single site as well as to the presence of neighboring sites. These mechanisms are discussed in Sec. VI.

VI. DISCUSSION

A. Microscopic mechanisms

1. *Scattering from a single site*

Electron scattering leading to the excitation of intramolecular, rotational, and translational vibrations of a molecular site can be divided as in the gas phase into direct[40] and resonant processes.[41] The direct process arises from the dependence on position, orientation, and internuclear separation of the electron–molecular-site interaction potential. It is described asymptotically by a single-center expansion leading to dipole, quadrupole, and polarization, etc., interactions and results in a smooth behavior of the cross section as a function of the incident energy.[42] The resonant process proceeds via the formation of a transient anion state characterized by the symmetry of the molecular site. Beside their occurrence at a particular energy, resonances are also characterized by an energy width for decay or lifetime. This effective interaction is of short range and so is expected to contribute mainly to the isotropic component of the SPUL in the two-stream model.

Direct process for vibrational excitation of H_2O has been calculated in the first Born approximation.[43] In this treatment the dipole and polarization terms are found to contribute mainly to the cross sections below 10 eV, reaching gradually a maximum around 1 eV. The quadrupole contribution is more flat and dominates above 10 eV. The differential cross sections are enhanced in the range of small scattering angle due to the long-range character of the dipole and polarization interactions, with a corresponding angular range becoming narrower as a function of increasing incident energy. In the present analysis, this is taken into account by the anisotropic or small-angle component of the SPUL. In counterpart, the quadrupole contribution provides an isotropic angular behavior to the differential cross sections, and so is represented by the isotropic or large-angle component of the SPUL. Rotational excitation by the direct process occurs as a result of a torque which arises from the electron field acting on the molecule. Calculations for H_2O molecule show[44] that the $00 \rightarrow 01$ rotational transition is by far the dominant excitation and is well described by the first Born approximation. The associated cross section is found to decrease rapidly from 1 to 10 eV incident energy. The differential cross sections obtained from calculations[44] as well as extracted from experimental measurements[45] are observed to be strongly peaked for small scattering angle. Hence, one expects generally that librational excitations should be characterized by a strong coefficient of angular anisotropy.

Two families of resonances are usually encountered in the gas phase:[41,46] single-particle or shape resonances and two-particle one-hole or core-excited resonances. For shape resonances the lifetime is generally of the or-

der of the molecular vibration (i.e., less than 10^{-14} sec), so they decay preferably into vibrational levels of the ground state. For core-excited resonances whose parent excited state is a closed channel for the resonance decay (i.e., Feshbach resonances), the lifetime is long (i.e., greater than 10^{-14} sec) thus providing sufficient time for vibrational excitation and dissociation of a molecule.

For the H_2O molecule in its ground state $(1a_1)^2(2a_1)^2(1b_2)^2(3a_1)^2(1b_1)^2, {}^1A_1$ the addition of an electron in the $(4a_1)$ or $(2b_2)$ next vacant antibonding orbital yields the formation of a $^2A_1$ or $^2B_2$ anion state, respectively. In the calculation of Claydon *et al.*,[47] it has been proposed as a final result that the $^2A_1$ state should be in the 2–3-eV energy range and the $^2B_2$ state in the 6–7-eV energy range. Later on, measurements of the elastic and vibrational (i.e., bending and stretching modes) cross sections performed in the gas phase revealed a strong enhancement at threshold[48,49] and a broad feature in the 6–8-eV energy range.[48] By comparing these measurements with cross section calculations applied for individual symmetry of the molecule, Jain and Thompson[50] were able to identify finally the role of the B_2 symmetry around 7 eV and that of the A_1 symmetry below 2 eV.

The first core-excited resonances in H_2O are formed when two electrons occupy the first Rydberg orbital

TABLE I. Cross sections as a function of the incident energy E_0 (eV) for electrons elastically scattered and exciting vibrational modes (ν_i) in amorphous ice at 14 K. $h\nu$, excitation energy of a mode (meV); δ, full width at half maximum (meV); σ, cross section per scatterer (10^{-17} cm^2); γ, coefficient of angular anisotropy.

	Excitation modes									
	Elastic		ν'_T		ν''_T		ν'_L		ν''_L	
	$h\nu$	(δ)	$h\nu$	(δ)	$h\nu$	(δ)	$h\nu$	(δ)	$h\nu$	(δ)
E_0 (eV)	σ	(γ)	σ	(γ)	σ	(γ)	σ	(γ)	σ	(γ)
1.7	0	(0)	10		25	(24)	62	(30)	95	(40)
	2.97	(0)	0		2.79	(0.55)	1.21	(0.70)	4.12	(0.75)
3.2	0	(0)	10		24	(25)	62	(30)	95	(38)
	2.22	(0)	0		1.33	(0.25)	0.98	(0.75)	2.91	(0.85)
5.2	0	(0)	10		24	(24)	62	(30)	95	(40)
	3.34	(0)	0		1.48	(0.30)	0.81	(0.60)	3.15	(0.90)
7.2	0	(0)	10		24	(25)	62	(30)	95	(40)
	3.45	(0)	0		1.66	(0.30)	1.13	(0.65)	3.99	(0.92)
9.2	0	(0)	10	(0)	26	(25)	62	(30)	93	(40)
	2.16	(0)	0.15	(0)	0.98	(0.30)	1.23	(0.70)	2.85	(0.94)
11.2	0	(0)	10	(0)	27	(25)	62	(30)	91	(40)
	2.39	(0)	0.25	(0)	0.95	(0.50)	0.89	(0.70)	1.91	(0.95)
13.2	0	(0)	10	(0)	25	(25)	62	(30)	93	(38)
	3.39	(0)	0.31	(0)	1.23	(0.50)	1.08	(0.70)	2.08	(0.95)
15.2	0	(0)	10	(0)	25	(25)	62	(30)	93	(40)
	3.58	(0)	0.36	(0)	1.19	(0.50)	1.29	(0.85)	2.27	(0.97)
17.2	0	(0)	10	(0)	25	(25)	60	(28)	90	(40)
	2.00	(0)	0.18	(0)	1.41	(0.80)	1.17	(0.95)	2.41	(0.98)

	ν_2		$\nu_{1,3}$		ν_3		$\nu_{1,3}+\nu_L$		$2(\nu_{1,3})$		Others	
	$h\nu$	(δ)	$h\nu$	(δ)	$h\nu$	(δ)	$h\nu$	(δ)	$h\nu$	(δ)	$h\nu$	(δ)
E_0 (eV)	σ	(γ)	σ	(γ)	σ	(γ)	σ	(γ)	σ	(γ)	σ	(γ)
1.7	205	(20)	422	(50)	460	(5)	500	(50)	850		> 900	
	0.29	(0.15)	0.61	(0.10)	0.04	(0.10)	0.10	(0.10)	0		0	
3.2	205	(20)	422	(50)	460	(5)	500	(50)	850		> 900	
	0.21	(0.25)	0.53	(0.10)	0.05	(0.10)	0.07	(0.10)	0		0	
5.2	205	(18)	422	(50)	460	(5)	500	(50)	850	(70)	> 900	
	0.25	(0.30)	0.67	(0.20)	0.07	(0.20)	0.16	(0.20)	0.05	(0.20)	0.17	
7.2	205	(11)	425	(50)	460	(5)	500	(40)	840	(80)	> 900	
	0.33	(0.60)	1.11	(0.35)	0.11	(0.30)	0.26	(0.25)	0.17	(0.20)	0.07	
9.2	205	(11)	430	(50)	460	(5)	500	(40)	830	(90)	> 900	
	0.33	(0.80)	1.03	(0.34)	0.07	(0.60)	0.22	(0.50)	0.22	(0.20)	0.59	
11.2	205	(11)	423	(50)	460	(5)	500	(40)	830	(120)	> 900	
	0.29	(0.90)	0.74	(0.55)	0.02	(0.50)	0.04	(0.50)	0.12	(0.20)	0.64	
13.2	207	(15)	420	(50)	462	(5)	500		830	(120)	> 900	
	0.34	(0.90)	0.70	(0.60)	0.02	(0.50)	0		0.10	(0.20)	1.03	
15.2	205	(15)	419	(50)	462		500		830	(120)	> 900	
	0.35	(0.95)	0.70	(0.70)	0		0		0.03	(0.20)	2.17	
17.2	205	(15)	418	(45)	462		500		830	(120)	> 900	
	0.39	(0.98	0.54	(0.80)	0		0		0.02	(0.20)	3.61	

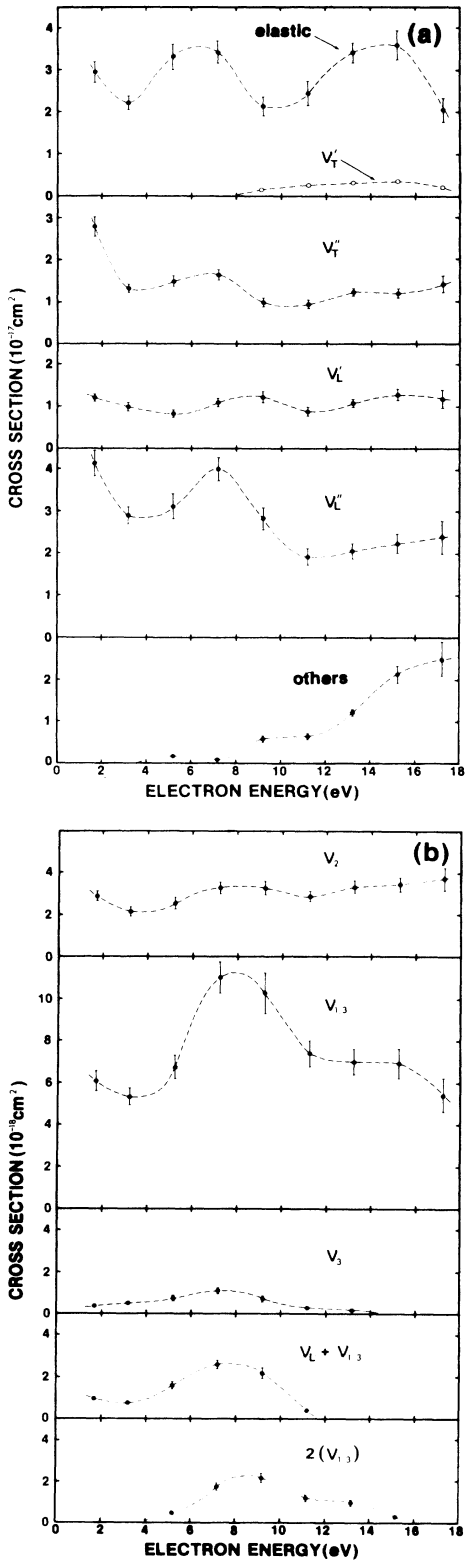

FIG. 4. Energy dependence of the elastic and vibrational electron scattering cross sections per scatterer in amorphous ice derived from the two-stream analysis of the energy-loss spectra of Fig. 2. The bottom curve in (a) represents the cross section ascribed mainly to the sum of electronic excitations. The numerical values of all cross sections are listed in Table I.

$(4a_1)$ with the positive core $\cdots(1b_2)^2(3a_1)^2(1b_1)$, $\cdots(1b_2)^2(3a_1)(1b_1)^2$, or $\cdots(1b_2)(3a_1)^2(1b_1)^2$. This results in the anion state of symmetry $^2B_1$, $^2A_1$, or $^2B_2$, respectively. In the gas phase these states are known to be repulsive; they have been identified and located around 6.5 eV for $^2B_1$, 8.6 eV for $^2A_1$, and 11.8 eV for $^2B_2$ by measuring the dissociative attachment cross section for H^-,[51–53] O^-,[52,53] and OH^- production.[52,53] Out of these, the $^2B_1$ state is the dominant process in the total dissociative attachment cross section. Other core-excited resonances associated with Rydberg states that arise from the promotion of a core electron to $3p,3d,4s,\ldots$ orbitals of the united atom have also been found to occur in the 9–12-eV energy range by electron transmission spectroscopy.[54] But since their cross section seems small and their decay channels are uncertain, they will not be considered further.

2. *Scattering from multiple sites*

In addition to the interactions already taking place between the film constituents (i.e., electrostatic, van der Waals), which could modify the ground state of a molecule, the presence of other scattering sites can yield two types of microscopic effects included intrinsically in our cross sections. One is the interference and coherent multiple scattering taking place between sites due to the quantum nature of the electron and the other concerns the modification brought to the scattering property of a site by the overlapping of the scattering potentials. The former effect is present even in the absence of overlapping, while the latter is apparent through virtual and real excitations of the surrounding medium. The virtual excitations originating particularly from the averaged electronic polarization has been addressed in Sec. II, when we introduced the real part of the constant complex potential V_p. Let us first look at the interference effects and then examine the consequences of overlapping of the interaction potentials especially in connection with resonant scattering.

The lowest order in a microscopic description of electron scattering in a condensed medium is the single-event contribution. Here the scattered amplitude is the coherent sum of amplitudes originating from individual site whereas the sum of amplitudes multiply scattered from different sites is considered negligible. This description is expected to be meaningful when the average distance between scattering events (i.e., MFP) is large in comparison with the de Broglie wavelength of the electron. This condition is also sufficient for the validation of a Boltzmann equation. Hence, the differential scattering cross section per unit solid angle $d\Omega$ and unit energy interval dE for a particle of mass m and wave-vector state $|\mathbf{k}_0\rangle$ to be scattered into the state $|\mathbf{k}\rangle$ can be given by[55,56]

$$\frac{d^2\sigma}{d\Omega dE}=\frac{1}{\hbar}\frac{|\mathbf{k}|}{|\mathbf{k}_0|}\left[\frac{m}{2\pi\hbar^2}\right]^2|V_{\mathbf{K}}|^2S(\mathbf{K},\omega)\,. \tag{6.1a}$$

The energy of the particle transferred to the medium is $\hbar\omega$ whereas the momentum transfer is $\hbar\mathbf{K}=\hbar\mathbf{k}_0-\hbar\mathbf{k}$. Thus the cross section can be separated into a term

$|V_{\mathbf{K}}|^2$ (i.e., Born differential cross section) associated with scattering originating from a site and into a dynamical structure factor term $S(\mathbf{K},\omega)$. This latter is related to the static as well as the dynamical correlation between sites in a condensed medium by the relation[55,56]

$$S(\mathbf{K},\omega)=\frac{N}{2\pi}\int dt\,\exp(-i\omega t)\int d^3x\,\exp(i\mathbf{K}\cdot\mathbf{x})G(\mathbf{x},t)\ , \tag{6.1b}$$

where $G(\mathbf{x},t)$ is defined as the space-time pair-correlation function. The instantaneous part of this function $G(\mathbf{x},0)$ (i.e., static approximation) applies to the sum of elastic and quasielastic scattering of x-rays in solids, liquids, and gases.[19] In the context of an amorphous medium, the spatial range of $G(\mathbf{x},0)$ can better define the size of the effective volume introduced in Sec. II and beyond which interference effects can be neglected. In the elastic case (i.e., $\omega=0$), if multiple scattering within a molecular site is partially summed, the Born amplitude can then be replaced by the T-matrix transition amplitude[57] and the factorization corresponding to (6.1) should represent more closely the behavior of the extracted elastic cross section. If time dependence is allowed for the pair-distribution function, the degree of correlation is expected to be further reduced. Accordingly, the cross sections for $\omega\neq 0$ associated to nuclear excitation modes should be less sensitive to the structure of the medium. In the limit where the excitation modes are uncorrelated, such as weakly coupled local oscillators or localized modes induced by disorder, the transferred energy is localized and interference effects similar to those occurring in the elastic cross section cannot arise in the inelastic cross sections. Hence, the various nuclear vibrational modes in amorphous ice, especially the intramolecular modes which are strongly coupled by hydrogen bonding but localized by disorder, are expected to be almost independent of the structure of the medium.

Owing to the overlapping of the electron-molecule interaction potentials in the condensed phase, a resonance process is also coupled with various longitudinal polarization modes (α) of the surrounding medium. From the point of view of these latters, the transient anion state is seen as a time-dependent perturbation with a resonance energy related to a transition time (τ_s) to go from the neutral ground state to the anion state and by an intrinsic width or lifetime for decay (τ_r). Out of the numerous models aimed at estimating the polarization energy of an extra charge in a dielectric, the molecular-ion model developed by Duke *et al.*[58] proved to be useful for the discussion of a transient anion state embedded in a medium.[7,59] In this model when $\hbar/\tau_s < E_\alpha(q)$, where $E_\alpha(q)$ is the energy of a longitudinal polarization mode, we are in the adiabatic limit and the system goes from the neutral ground state to the relaxed anion state. Otherwise, when $\hbar/\tau_s > E_\alpha(q)$, we are in the sudden approximation limit, and if the contribution to the polarization energy brought about by a longitudinal polarization mode is much smaller or greater than $E_\alpha(q)$, a mode is classified as contributing either to the shift or to the broadening of a resonance, respectively. In this latter case, the energy transferred to the medium is favored only in those modes which are allowed to evolve significantly during the resonance lifetime.[59] How the energy, lifetime, symmetry, and the decaying channels of a particular resonance are to be modified in this context constitutes a major step in the understanding of the energy dependence of the various cross sections.

B. Cross section analysis

1. *Intramolecular-vibrational cross sections*

Because of the difficulty in separating the stretching region into a symmetric ν_1 and an asymmetric ν_3 modes, a single Gaussian distribution of about 50 meV FWHM is used to represent both modes at all energies (Table I). However, around 7–9 eV of incident energy, it is necessary to shift this distribution toward higher energy loss where a characteristic enhancement occurs in the cross section as shown in Fig. 4(b). It is noticeable that despite the small value of the SPUL involved a similar enhancement is found also for the overtone $2(\nu_{1,3})$ in the same energy range. This enhancement can be explained mainly by the presence of the shape resonance associated with the $^2B_2$ anion state. Owing to the distribution induced on the ground state of the H_2O molecule by hydrogen bonding, this latter is not expected to occur at the gas-phase energy and to retain the same lifetime. Furthermore, the electronic polarization modes are expected to lower the resonance energy and to contribute to its width through inhomogeneous distribution of polarization energies. We observe the $^2B_2$ anion state to lie effectively at higher energy in the condensed phase. Considering the observed energy-loss shift and the vibrational ordering derived from the gas phase[27,28] as well as the Raman spectra of ice VIII,[31] it should decay preferably in the asymmetric stretching mode ν_3. In counterpart, the coefficient of angular anisotropy $\gamma_{1,3}$ (Table I), is found to increase steadily from low to high incident energy. This indicates that there is a contribution to the cross section due to long-range interaction. This latter is expected to originate particularly from the dipolar term and to explain the small rise below 3 eV.

For the bending mode ν_2 a fixed energy-loss distribution with a smaller FWHM around 7–9 eV is utilized (Table I). The behavior of the cross section shown in Fig. 4(b) is similar to the stretching modes with the small rise at low energy and a slight vibrational enhancement at $^2B_2$ resonance position. The coefficient of angular anisotropy γ_2 (Table I) follows the same general trend as for the stretching modes but is on the average 1.5 greater, thus indicating an increased contribution of the long-range interaction to the cross section. These results are consistent with gas-phase data where resonance enhancement is found more pronounced in the stretching than in the bending-mode cross section[48,50] and where the dipole interaction[4] results in a larger contribution for the bending-mode cross section.[43]

2. *Intermolecular-vibrational cross sections*

The librational phonon modes are conveniently described by two energy distributions of almost constant

energy-loss position $h\nu'_L \cong 62$ meV $h\nu''_L \cong 95$ meV and FWHM as a function of the incident energy (Table I). As can be seen in Fig. 4(a), the cross section of the higher energy-loss mode ν''_L is 2–3 times more intense than that of the lower mode ν'_L. Both are characterized by a rise at low energy followed by an enhancement around 7 eV for ν''_L and a broader feature around 9 eV for ν'_L. It is this latter behavior which allows the distributions to be resolved directly in the energy-loss spectra at 9 eV of incident energy in Fig. 2(b). The coefficients of angular anisotropy γ'_L, γ''_L (Table I) are high (i.e., greater than 0.6) at all energies for both modes in comparison with the intramolecular-vibrational modes. This indicates that the direct process via the permanent dipole of H_2O contributes largely, over the entire energy range, to the excitation of the librons as well as to the rise in the cross sections toward low energy.

The translational phonon mode is represented by a distribution centered around $h\nu''_T \cong 25$ meV (Table I). Addition of a mode ν'_T contributes to improve the fit, but will not be considered further because of a certain incertitude remaining in its determination. The cross section of the mode ν''_T shown in Fig. 4(a) presents a strong rise at low energy and a feature very similar to the mode ν''_L around 7.0 eV. As a function of increasing energy the coefficient of angular anisotropy γ''_T (Table I) is found to decrease from a relatively high value reaching a minimum around 3 eV and then to increase steadily. Hence, direct excitation which arises from the gradient of the field of the scattered electron should be important especially at low incident energy where the strong rise occurs.

While the general trend of these cross sections can be ascribed to direct processes, the features around 7–9 eV is attributed to the formation of molecular anion states. With this respect, we have proposed recently[59] a mechanism by which a transient anion state can transfer energy to the vibrational modes of the surrounding medium via the long-range dipole interaction. When applied to amorphous ice, our model suggests that short-lived resonances (e.g., shape resonances) are restricted to decay into intramolecular-vibrational modes pertaining to the anion site as in the gas phase. In counterpart, longer-lived resonances (e.g., core-excited resonances) can decay into intermolecular-vibrational modes of the surrounding molecules as well as into intramolecular modes at the anion site. However, owing to the general perturbation suffered by Rydberg states in the condensed phase, core-excited resonances originating from the conditional existence of these states (i.e., parent states) are not at all guaranteed. For instance, in amorphous ice only a broad feature around 8 eV can be clearly resolved in the HREEL (Ref. 60) and ultraviolet absorption spectra.[38] This is identified as the excitation of the $^{3,1}B_1$ Rydberg state located around 7.5 eV in the gas phase.[61] It originates from the promotion of a $(1b_1)$ electron to the first empty orbital $(4a_1)$ which is correlated to a Rydberg orbital of the united-atom description. The promotion of the other core electrons into the same empty orbital yields the $^{3,1}A_1$ state at 9.6 eV and the $^{3,1}B_2$ state at 11.5 eV in the gas phase.[61] However, they are expected to be progressively more perturbed in the amorphous phase due to their increasing Rydberg radius. Thus, only the anion state $^2B_1$ and to a lesser extent the $^2A_1$ are likely to occur in a molecular site at an energy associated to their parent state. Similarly to shape resonance, the electronic polarization is expected to shift the resonance at lower energy and to contribute to the broadening. Hence, the maxima around 7 eV in the ν''_L, ν''_T modes and around 9 eV in the ν'_L mode could arise from the anion states $^2B_1$ and $^2A_1$ observed in the gas phase at 6.5 and 8.6 eV, respectively.[51–53] The excitation of these intermolecular modes is characterized by the anion site remaining in its neutral ground state. However, excitation of intramolecular vibrational modes as a final state is always possible and should allow one to observe the resonances in decay channels associated also to combination modes. Incidently, the magnitude and position of the maximum in the cross section for the combination of a libron with the stretching modes (i.e., $\nu_L + \nu_{1,3}$) shown in Fig. 4(b) seem to be consistent with this assertion.

3. *Elastic cross section*

The elastic cross section illustrated in Fig. 4(a) corresponds to the large-angle component (i.e., $2Q_{re}$). It reveals a rise at low energy and two broad structures whose maxima are located at $E_0 = 6$ and 14.5 eV. For the incident energy 1 eV $< E_0 <$ 18 eV, the electron MFP (Ref. 16) is 3 to 10 times larger than the de Broglie wavelength of the electron, and the module of the maximum wave-vector transfer $|\mathbf{K}_{\max}| = 2|\mathbf{k}_0|$ lies from 1 to 4.3 Å^{-1}, respectively. In this latter range, the structure factor of amorphous ice at 10 K,[37] being characterized by two well-developed structures located at $|\mathbf{K}|_1 = 2$ Å^{-1} and $|\mathbf{K}|_2 = 3.1$ Å^{-1}, suggests *a priori* that the features in the cross section could originate from interference effects. In fact, the cross section for an electron elastically scattered from a disordered medium can be obtained in the single-event approximation from expression (6.1a) as

$$Q_{te} = \frac{1}{\hbar}\left[\frac{m}{2\pi\hbar^2}\right]^2 \int_0^{\pi}\int_0^{2\pi} |V(|\mathbf{K}|)|^2 S(|\mathbf{K}|) \times \sin\theta\, d\theta\, d\phi \,, \tag{6.2a}$$

where

$$|\mathbf{K}| = [2(1-\cos\theta)]^{1/2}|\mathbf{k}_0| \tag{6.2b}$$

and θ is the angle between the incident $\mathbf{k}_0$ and scattered $\mathbf{k}$ electron wave vector. Considering the energy-conservation condition (i.e., $|\mathbf{k}_0| = |\mathbf{k}|$) only $|\mathbf{K}|$ instead of $\mathbf{K}$ is necessary in Eqs. (6.2) provided that the medium as well as the individual scattering site are orientationally disordered. For a fixed incident energy (i.e., $|\mathbf{k}_0|$), $S(|\mathbf{K}|)$ depends only on θ according to the relation (6.2b). Thus each maximum in $S(|\mathbf{K}|)$ (e.g., $|\mathbf{K}|_1$, $|\mathbf{K}|_2$) can be seen to describe as functions of the incident energy a continuous trajectory in the $(|\mathbf{k}_0|, \theta)$ plane. How maxima in $S(|\mathbf{K}|)$ can yield maxima at specific energies in the cross section can be visualized with the following considerations.

For a spatial range of the electron-site scattering potential much smaller than the de Broglie wavelength of the electron, the dependence on θ is to arise mainly from the $S(|\mathbf{K}|)$ factor in (6.2a). In the limit where $V(|\mathbf{K}|)$ can be considered a constant (i.e., for an isotropic scattering cross section of a site), the expression (6.2a) simplifies to

$$Q_{te}=\frac{2\pi}{\hbar}\left[\frac{m}{2\pi\hbar^2}\right]^2 |V|^2\int_0^{\pi} S(|\mathbf{K}|)\sin\theta\, d\theta\ . \tag{6.3}$$

By performing the angular integration as a function of the incident energy, a maximum should occur in Q_{te} whenever the trajectory followed by a maximum $|\mathbf{K}|_i$ in the $(|\mathbf{k}_0|,\theta)$ plane cross the line at $\theta=\pi/2$ defined by the maximum value of the modulating factor $\sin\theta$. Otherwise, if the term $|V(|\mathbf{K}|)|^2$ cannot be factorized out, one can define a similar effective line $\theta=\theta_{\text{eff}}(|\mathbf{k}_0|)$. Thus with (6.2b) we have for a feature $|\mathbf{K}|_i$ the relation

$$|\mathbf{K}|_i=[2(1-\cos\theta_{\text{eff}})]^{1/2}(2mE_{0i})^{1/2}/\hbar\ . \tag{6.4}$$

Furthermore, for θ_{eff} weakly dependent on $|\mathbf{k}_0|$ we should have between two features located at $|\mathbf{K}|_i$ and $|\mathbf{K}|_j$ in $S(|\mathbf{K}|)$ the ratio

$$|\mathbf{K}|_i/|\mathbf{K}|_j\simeq(E_{0i}/E_{0j})^{1/2}\ . \tag{6.5}$$

Applying (6.5) with $2Q_{re}$ as Q_{te}, since interference effects are not likely to arise from small $\mathbf{K}$ in this energy range, we obtain $(E_{01}/E_{02})^{1/2}=0.643$ in close agreement with $|\mathbf{K}|_1/|\mathbf{K}|_2=0.645$ from $S(|\mathbf{K}|)$. Moreover, using (6.4) a value of 106° can be deduced for θ_{eff}.

The rise in the cross section at low energy not being accounted for by the structure factor could be of dipolar or resonance origin. Since the dipole interaction is of long range, its effect should appear mainly in the small-angle component (i.e., Q_{fe}). Hence, the extracted large-angle component $2Q_{re}$ should be correlated to a threshold effect associated with the $^2A_1$ anion state located around 2 eV.[48–50] As demonstrated in the description of resonances in the fixed nuclei limit[62] and for short-range potentials, a $l=0$ anion state near threshold yields a virtual state (i.e., "bound state" that slipped out of an insufficiently bonding potential). However, in presence of a strong long-range potential such as that generated by the dipole moment[62] of the H_2O molecule the virtual state is destroyed, and instead a weakly bound state is maintained just below threshold. In either case, for a $l=0$ anion state even reasonably above threshold, a large enhancement of the cross section at threshold should result.

4. *Electronic cross section*

The remaining cross section, once the analysis of the vibrational spectra is completed, is shown at the bottom of Fig. 4(b). It corresponds essentially to the imaginary part Γ of the electron self-energy introduced in Sec. II. This cross section is significant only above the electronic excitation threshold (i.e., 7.5 eV). At 17 eV, it accounts for about 37% of the total inelastic cross section. While in the 7.5–17-eV range the residual cross section is likely to arise from various electronic excitation and ionization processes, the small value around 5.2 eV could originate from vibrational excitations occurring outside the probed energy-loss range and from dissociative attachment processes.

VII. CONCLUSION

We have shown that under reasonable experimental conditions, it is possible to extract absolute cross-section values for electron scattering in a disordered medium by using a two-stream analysis of HREEL spectra recorded on vacuum-deposited films of sufficiently high thickness. Incoherent elastic and inelastic electron collisions are included as well as overlapping between broad energy-loss features. Although the angular distribution of a scattering event is simply described by a coefficient of angular anisotropy, this latter can simulate effectively the long-range interaction (e.g., dipole scattering) which is an important process in electron-H_2O scattering. When applied to amorphous ice films, this analysis is able to provide cross sections for the major energy losses along with their mean excitation energies and FWHM values. The energy-dependent cross sections so extracted include intrinsically coherent scattering (e.g., interference effects) originating from a single site and from the presence of neighboring sites. While the former can result in resonant scattering similar to the gas phase, the latter can be described in lowest order by the dynamical structure factor as long as the MFP of the electron is much larger than its de Broglie wavelength. According to the determined total cross section, this condition seems to be reasonably fulfilled in the present study.

ACKNOWLEDGMENTS

We wish to thank J. P. Corbeil and T. Buhagiar for technical assistance in the calculations. Financial support from the Medical Research Council of Canada is gratefully acknowledged.

APPENDIX: DERIVATION OF ANALYTICAL EXPRESSIONS FOR THE ELASTIC AND INELASTIC BACKSCATTERED INTENSITY

The backscattered current-density distribution $J_{\infty}^{T}(0,E)$ given by the expression (2.7) includes the effect of angular anisotropy in a scattering event as well as the transmission at the potential-barrier interface, both in all orders of scattering. Its Fourier transform as given in (2.7), i.e.,

$$J_{\infty}^{T}(0,s)=\frac{I(0,s)TR_{\infty}(0,s)}{1-(1-T)R_{\infty}(0,s)} \tag{A1a}$$

with (2.3b) rewritten as

$$R_{\infty}(0,s)=\frac{1-\{1-2Q_r(s)/[\alpha-Q_f(s)]\}^{1/2}}{1+\{1-2Q_r(s)/[\alpha-Q_f(s)]\}^{1/2}}\ , \tag{A1b}$$

is a continuous function of the independent variables $Q_r(s)$ and $Q_f(s)$. The expressions for the elastic and inelastic backscattered intensities in order of increasing

number of inelastic events can be obtained in a systematic manner by expanding $J^T_\infty(0,s)$ into a Taylor series about the points $Q_{re}\equiv Q_r(E=E')$, $Q_{fe}\equiv Q_f(E=E')$. With $Q_r(s)=Q_{re}+Q_{ri}(s)$ and $Q_f(s)=Q_{fe}+Q_{fi}(s)$, the series truncated after the first inelastic event reads

$$J^T_\infty(0,s)=[J^T_\infty(0,s)]_{Q_{re},Q_{fe}} + \frac{Q_{ri}(s)}{\alpha}\left[\frac{\partial J^T_\infty(0,s)}{\partial Q_r(s)/\alpha}\right]_{Q_{re},Q_{fe}} + \frac{Q_{fi}(s)}{\alpha}\left[\frac{\partial J^T_\infty(0,s)}{\partial Q_f(s)/\alpha}\right]_{Q_{re},Q_{fe}} . \quad \text{(A2)}$$

The first term represents the elastic backscattered intensity and using expressions (A1) is readily given by

$$[J^T_\infty(0,s)]_{Q_{re},Q_{fe}}\equiv J^T_{\infty e}=\frac{I_0 T R_{\infty e}}{1-(1-T)R_{\infty e}} , \quad \text{(A3a)}$$

where

$$R_{\infty e}\equiv[R_\infty(0,s)]_{Q_{re},Q_{fe}}=\frac{1-[1-2Q_{re}/(\alpha-Q_{fe})]^{1/2}}{1+[1-2Q_{re}/(\alpha-Q_{fe})]^{1/2}} \quad \text{(A3b)}$$

is the intrinsic elastic reflectivity for the semi-infinite medium.

The second and third terms in the series (A2) are the inelastic backscattered intensities related to the large- and small-angle inelastic scattering, respectively. The effect of the transmission at the potential-barrier interface and the intrinsic elastic multiple scattering can be separated into distinct factors by applying the chain rule on the partial derivative as

$$\left[\frac{\partial J^T_\infty(0,s)}{\partial[Q_{r,f}(s)/\alpha]}\right]_{Q_{re},Q_{fe}} = \left[\left[\frac{\partial J^T_\infty(0,s)}{\partial R_\infty(0,s)}\right]\left[\frac{\partial R_\infty(0,s)}{\partial[Q_{r,f}(s)/\alpha]}\right]\right]_{Q_{re},Q_{fe}} . \quad \text{(A4)}$$

The first factor in the right-hand side of this equation is explicitly given by

$$\frac{\partial J^T_\infty(0,s)}{\partial R_\infty(0,s)}=\frac{I(0,s)T}{[1-(1-T)R_\infty(0,s)]^2} \quad \text{(A5)}$$

and represents the effect of the barrier. The second factor for large- or small-angle scattering when evaluated along lines similar to Sec. IV in I are given by

$$\frac{\partial R_\infty(0,s)}{\partial[Q_r(s)/\alpha]}=\left[\frac{1}{1-Q_f(s)/\alpha-2Q_r(s)/\alpha}\right]\times\left[\frac{1-R^2_\infty(0,s)}{2}\right] \quad \text{(A6a)}$$

and

$$\frac{\partial R_\infty(0,s)}{\partial[Q_f(s)/\alpha]}=\left[\frac{Q_r(s)/\alpha}{1-Q_f(s)/\alpha}\right]\times\left[\frac{1}{1-Q_f(s)/\alpha-2Q_r(s)/\alpha}\right]\times\left[\frac{1-R^2_\infty(0,s)}{2}\right] , \quad \text{(A6b)}$$

respectively.

The combination of (A6) with (A5) evaluated at the points Q_{re},Q_{fe}, once inserted in (A2) yields explicitly for the inelastic first-order term

$$J^T_i(0,s)=\frac{I(0,s)T}{[1-(1-T)R_{\infty e}]^2}\times\left[\frac{Q_{ri}(s)}{\alpha_i}+\frac{Q_{fi}(s)}{\alpha_i}\left[\frac{Q_{re}}{\alpha-Q_{fe}}\right]\right]\times\left[\frac{1-R^2_{\infty e}}{2}\right] , \quad \text{(A7)}$$

where $R_{\infty e}$ is given by (A3b) and $\alpha_i\equiv\alpha-Q_{fe}-2Q_{re}$ is the total inelastic SPUL. Finally, by performing the inverse Fourier transform as prescribed by (2.7) with $I(0,s)=I_0$ [i.e., $I(E-E')=I_0\delta(E'-E_0)$], we get for the inelastic backscattered intensity

$$J^T_i(0,E)=\frac{I_0 T}{[1-(1-T)R_{\infty e}]^2}\times\left[\frac{Q_{ri}(E-E_0)}{\alpha_i}+\frac{Q_{fi}(E-E_0)}{\alpha_i}\times\left[\frac{2R_{\infty e}}{(1+R_{\infty e})^2}\right]\right]\times\left[\frac{1-R^2_{\infty e}}{2}\right] , \quad \text{(A8)}$$

where using (A1b) the factor $Q_{re}/(\alpha-Q_{fe})$ is expressed in terms of $R_{\infty e}$.

---

[1]For a review see *Electron Beam Interactions in Solids for Microscopy, Microanalysis, and Microlithography*, edited by D. F. Kyser, H. Niedrig, D. E. Newbury, and R. Shimizu (Scanning Electron Microscopy, Inc., AMF O'Hare, Illinois, 1984); A. L. Tofterup, Phys. Rev. B **32**, 2808 (1985); C. J. Powell, Scanning Electron Microsc. **4**, 1649 (1984) and references cited therein.

[2]For a comprehensive review of the problems in radiation physics, see M. Inokuti, in *Applied Atomic Collision Physics*, Vol. 4 of *Condensed Phases*, edited by S. Datz (Academic, New York, 1983), pp. 179–236.

[3]T. Hibma, P. Pfluger, and H. R. Zeller, in *Electronic Properties of Polymers and Related Compounds*, Vol. 63 of *Springer Series of Solid-State Sciences* (Springer, New York, 1985).

[4]H. Ibach and D. L. Mills, *Electron Energy Loss Spectroscopy and Surface Vibrations* (Academic, New York, 1982); in *Vibrational Spectroscopy of Adsorbates*, edited by R. F. Willis (Springer-Verlag, New York, 1980).

[5]For a review see *Electron-Molecule Interaction and their Applications*, edited by L. G. Christophorou (Academic, Orlando, 1984), Vol. 1.

[6]L. Sanche and M. Michaud, Phys. Rev. B **30**, 6078 (1984); in *Resonances in Electron-Molecule Scattering van der Waals Complexes, and Reactive Chemical Dynamics*, edited by Donald G. Truhlar (American Chemical Society, Washington, D.C., 1984), pp. 211–228 and references cited therein.

[7]L. Sanche, G. Perluzzo, and M. Michaud, J. Chem. Phys. **83**, 3837 (1985).

[8]R. Marsolais, M. Michaud, and L. Sanche, Phys. Rev. A **35**, 607 (1987).

[9]G. Bader, G. Perluzzo, L. G. Caron, and L. Sanche, Phys. Rev. B **26**, 6019 (1982); **30**, 78 (1984); L. G. Caron, G. Perluzzo, G. Bader, and L. Sanche, *ibid* **33**, 3027 (1986).

[10]G. Perluzzo, L. Sanche, C. Gaubert, and R. Baudoing, Phys. Rev. B **30**, 4292 (1984); G. Perluzzo, G. Bader, L. G. Caron, and L. Sanche, Phys. Rev. Lett. **55**, 545 (1985).

[11]L. Sanche, Phys. Rev. Lett. **53**, 1638 (1984); L. Sanche and L. Parenteau, J. Vac. Sci. Technol. A **4**, 1240 (1986).

[12]C. B. Duke and G. E. Laramore, Phys. Rev. B **2**, 4765 (1970); G. E. Laramore and C. B. Duke, *ibid.* **2**, 4783 (1970); V. Roundy and D. L. Mills, *ibid.* **5**, 1347 (1972); C. H. Li, S. Y. Tong, and D. L. Mills, *ibid.* **21**, 3057 (1980).

[13]S. Tougaard and P. Sigmund, Phys. Rev. B **25**, 4452 (1982) and references cited therein.

[14]M. Michaud and L. Sanche, Phys. Rev. B **30**, 6067 (1984) and references cited therein.

[15]B. Plenkiewicz, P. Plenkiewicz, G. Perluzzo, and J.-P. Jay-Gerin, Phys. Rev. B **32**, 1253 (1985); J.-P. Jay-Gerin, B. Plenkiewicz, P. Plenkiewicz, G. Perluzzo, and L. Sanche, Solid State Commun. **55**, 1115 (1985).

[16]M. Michaud and L. Sanche, preceding paper, Phys. Rev. A **36**, 4672 (1987).

[17]G. Bader, J. Chiasson, L. G. Caron, M. Michaud, G. Perluzzo, and L. Sanche (unpublished).

[18]L. Hedin and S. Lundqvist, Solid State Phys. **23**, 1 (1969).

[19]C. B. Duke, J. R. Anderson, and C. W. Tucker, Jr., Surf. Sci. **19**, 117 (1970); C. B. Duke and G. E. Laramore, Phys. Rev. B **3**, 3183 (1971).

[20]This expression is readily derived from the calculation of the attenuation of an electron plane wave in a medium with α_i to be identified as $1/\lambda_{ee}$ in Ref. 19.

[21]This V_p value is to be distinguished from the V_0 which is defined as the energy of the bottom of the conduction band which originates from coherent elastic multiple scattering between sites.

[22]U. Fano and J. A. Stephens, Phys. Rev. B **34**, 438 (1986).

[23]P. A. Wolff, Phys. Rev. **95**, 56 (1954).

[24]M. Michaud and L. Sanche, J. Vac. Sci. Technol. **17**, 274 (1980).

[25]A large number of studies aimed at characterizing the structural arrangement and chemical reactions of water molecules on surfaces use these particular scattering properties (e.g., Ref. 26). However, since we are interested in scattering within the bulk of amorphous ice, we must avoid this low-thickness regime.

[26]C. Nyberg, C. G. Tengstal, P. Uvdal, and S. Anderson, J. Electron Spectroc. Relat. Phenom. **38**, 299 (1986); M. Nishijima, K. Edamoto, Y. Kubota, and S. Tanaka, and M. Onchi, J. Chem. Phys. **84**, 6458 (1986); P. Schmeisser and J. E. Demuth, Phys. Rev. B **33**, 4233 (1986); P. A. Thiel, R. A. DePaola and F. M. Hoffman, J. Chem. Phys. **80**, 5326 (1984); F. Stucki, J. Anderson, and G. J. Lapeyre, Surf. Sci. **143**, 84 (1984); B. A. Sexton, *ibid.* **94**, 435 (1980); H. Ibach and S. Lehwald, *ibid.* **91**, 187 (1980); G. B. Fisher and J. L. Gland, *ibid.* **94**, 446 (1980).

[27]G. Herzberg, *Infrared and Raman Spectra of Polyatomic Molecules* (Van Nostrand Reinhold, New York, 1945).

[28]T. Shimanouchi, *Tables of Molecular Vibrational Frequencies Consolidated*, Natl. Bur. Stand. Ref. Data Ser., Natl. Bur. Stand (U.S.), Circ. No. 39, U.S. GPO, Washington, D.C., 1972), Vol. I.

[29]W. Hagen, A. G. G. M. Tielens, and J. M. Greenberg, Chem. Phys. **56**, 367 (1981); T. C. Sirakumar, S. A. Rice, and M. G. Sceats, J. Chem. Phys. **69**, 3468 (1978); J. R. Scherer and R. G. Snyder *ibid.* **67**, 4794 (1977); J. E. Bertie and S. M. Jacobs, *ibid.* **67**, 2445 (1977); M. J. Taylor and E. Whalley, *ibid.* **40**, 1660 (1964); J. E. Bertie and E. Whalley, *ibid.* **40**, 1637 (1964).

[30]S. I. Ikawa and S. Maeda, Spectrochim. Acta, Part A **24**, 655 (1968).

[31]P. T. T. Wong and E. Whalley, J. Chem. Phys. **64**, 2350 (1976).

[32]D. F. Coker, J. R. Reimers, and R. O. Watts, Aust. J. Phys. **35**, 623 (1982).

[33]M. S. Bergren and S. A. Rice, J. Chem. Phys. **77**, 583 (1982).

[34]J. R. Reimers and R. O. Watts, Chem. Phys. Lett. **94**, 222 (1983).

[35]J. Kruger and W. J. Ambs, J. Opt. Soc. Am. **49**, 1195 (1959).

[36]R. W. G. Wyckoff, *Crystal Structures*, 2nd ed. (Interscience, New York, 1963), p. 322.

[37]A. H. Narten, C. G. Venkatesh, and S. A. Rice, J. Chem. Phys. **64**, 1106 (1976).

[38]T. Shikaguchi, H. Onuki, and R. Onaka, J. Phys. Soc. Jpn. **42**, 152 (1977); M. Watanabe, H. Kitamura, and Y. Nakai, in *Vacuum Ultraviolet Radiation Physics*, edited by E. E. Koch, R. Haensel, and C. Kunz (Pergamon, New York, 1974), p. 70.

[39]B. Baron, D. Hoover, and F. Williams, J. Chem. Phys. **68**, 1997 (1978).

[40]K. Takayanagi, in *Electron-Molecule Collisions*, edited by I. Shimamura and K. Takayanagi (Plenum, New York, 1984), Chap. 1.

[41]For a review of electron resonances in gases, see G. J. Schulz, Rev. Mod. Phys. **45**, 378 (1973); **45**, 423 (1973); G. J. Schulz, in *Principle of Laser Plasmas*, edited by G. Bekefi (Wiley, New York, 1976), p. 33.

[42]K. Takayanagi, J. Phys. Soc. Jpn. **21**, 507 (1966).

[43]Y. Itikawa, J. Phys. Soc. Jpn. **36**, 1127 (1974).

[44]A. Jain and D. G. Thompson, J. Phys. B **16**, 3077 (1983).

[45]K. Jung, Th. Antoni, R. Müller, K. H. Kochem, and H. Erhardt, J. Phys. B **15**, 3535 (1982).

[46]H. S. Taylor, Adv. Chem. Phys. **18**, 91 (1970).

[47]C. R. Claydon, G. A. Segal, and H. S. Taylor, J. Chem. Phys. **54**, 3799 (1971).

[48]G. Seng and F. Linder, J. Phys. B **7**, L509 (1974); **9**, 2539 (1976).

[49]K. Rohr, J. Phys. B **10**, L735 (1977).

[50]A. Jain and D. G. Thompson, J. Phys. B **16**, L347 (1983).

[51]D. S. Belić, M. Landau, and R. I. Hall, J. Phys. B **14**, 175 (1981); S. Trajmar and R. I. Hall, J. Phys. B **7**, L458 (1974).

[52]M. Jungen, J. Vogt, and V. Staemmler, Chem. Phys. **37**, 49

(1979).
[53]C. E. Melton, J. Chem. Phys. **57**, 4218 (1972).
[54]L. Sanche and G. J. Schulz, J. Chem. Phys. **58**, 479 (1973).
[55]C. Kittel, *Quantum Theory of Solids* (Wiley, New York, 1963), Chap. 19.
[56]L. Van Hove, Phys. Rev. **95**, 249 (1954).
[57]J. R. Taylor, *Scattering Theory* (Wiley, New York, 1972), Chap. 8.
[58]C. B. Duke, W. R. Salaneck, T. J. Fabish, J. J. Ritsko, H. R. Thomas, and A. Paton, Phys. Rev. B **18**, 5717 (1978).
[59]M. Michaud and L. Sanche, Phys. Rev. Lett. **59**, 645 (1987).
[60]M. Michaud and L. Sanche (unpublished).
[61]A. Chutjian, R. I. Hall, and S. Trajmar, J. Chem. Phys. **63**, 892 (1975).
[62]W. Domcke, J. Phys. B **14**, 4889 (1981).